Journal of Applied Polymer Science

Polystyrene/Calcium Carbonate Nanocomposites Prepared by *In Situ* Polymerization in the Presence of Maleic Anhydride

Weihua Luo, Xingxing Liu, Limin Sun
Division of Polymer Materials and Engineering, College of Material Science and Engineering, Central South University of Forestry and Technology, Changsha 410004, China
Correspondence to: W. Luo (E-mail: lwh6803@163.com)

ABSTRACT: Polystyrene (PS)/calcium carbonate ($CaCO_3$) nanocomposites were prepared by *in situ* polymerization in the presence of maleic anhydride (MA). The composites were characterized by Fourier transform infrared spectra, gel permeation chromatography, differential scanning calorimetry, controlled stress rheometer, scanning electron microscope (SEM), small-angle X-ray scattering (SAXS), and mechanical test. Results show that the copolymer of styrene (St) and MA formed during the polymerization acts as a compatibilizer between PS and nanometer calcium carbonate (nano-$CaCO_3$) particles, resulting in an increase in the glass transition temperature of the composite. The complex modulus and the impact strength of the PS/nano-$CaCO_3$ composite show an increase with the addition of MA on account of the enhanced interfacial adhesion and the increased molecular weight. SEM and SAXS analyses indicate that a finer dispersion of nanoparticles and an increased homogeneity of the PS/nano-$CaCO_3$ composites are obtained with application of a small amount of MA. © 2012 Wiley Periodicals, Inc. J. Appl. Polym. Sci. 000: 000–000, 2012

KEYWORDS: composites; *in situ* polymerization; compatibilization; polystyrene; inorganic nanoparticles

Received 4 December 2010; accepted 22 February 2012; published online
DOI: 10.1002/app.37566

INTRODUCTION

Polymer/inorganic nanocomposites have attracted tremendous attention for their potential in improving polymer properties. The predicted potential of nanocomposites is not frequently achieved because of a low homogeneous distribution and a weak interfacial adhesion. Nanoparticles tend to aggregate for their high surface energy, and hence, how to get a nanometer-scale dispersion of nanoparticles is still a challenge for preparation of polymer/inorganic nanocomposites. Many approaches have been developed for preparing polymer/inorganic nanocomposites, such as melt mixing method,[1,2] solution method,[3,4] and *in situ* polymerization method.[5–11] Melt and solution mixing methods usually obtain a relatively poor dispersion of nanoparticles in the composite because of high viscosity of the melt and entanglements between macromolecules.[12] The *in situ* polymerization of monomers in the presence of nanofillers is a promising approach for a more homogeneous distribution because of the close contact of fillers and the polymer matrix during synthesis.[5,6] However, properties of the nanocomposite are still limited by the weak interaction between the nanoparticles and the polymer matrix. Many researches have been carried out on surface modification of nanoparticles to improve the interfacial adhesion[13–15]; however, these off-site methods may increase the cost of production.

In this work, polystyrene (PS)/nano-$CaCO_3$ *in situ* composites were prepared by polymerization of styrene (St) and maleic anhydride (MA) in the presence of nano-$CaCO_3$ particles. The dispersion of nanoparticles in the polymer matrix and the interfacial interaction between polymer and inorganic particles were investigated.

EXPERIMENTAL

Materials

St was obtained from Tianjin Damao Chemical Reagent Plant, Tianjin, China, and was distilled before use. MA was obtained from Tianjin Bodi Chemical Industry, Tianjin, China. The nanometer calcium carbonate (nano-$CaCO_3$) was supplied by Yanhua Chemical, Jiangmen, China, and has a specific surface area of 22 m^2/g and a mean particle diameter of 80 nm. It was dried at a temperature of 100°C for 4 h before use. Benzoyl peroxide (BPO) and poly (vinyl alcohol) (PVA) with a degree of polymerization of 1750 and a degree of saponification of 99% were purchased from Hunan Xiangzhong Chemical Reagent, Loudi, China. PVA (3 g) was dissolved in 179 mL of distilled

water at 80°C and then cooled to room temperature for later use.

Preparation of PS/Nano-$CaCO_3$ *In Situ* Composites

Into a 500-mL four-necked boiling flask, 3 g of nano-$CaCO_3$ was dispersed in 22 mL of St, and 0.5 g of BPO was added and dissolved by joggling the flask. Then 25 mL of PVA solution and 175 mL of distilled water were induced. The mixture was heated to 85°C with stirring at a rate of 200 rpm. After a definite time, MA was added. The polymerization was carried out at this temperature for 4 h. The product was filtered and washed with hot distilled water, then vacuum dried for 24 h at 70°C to remove MA monomer and PVA. By changing the addition time and the amount of MA, a series of PS/nano-$CaCO_3$ *in situ* composites with particle size ranging from 0.2 to 1.2 mm was obtained. The monomer conversion was determined by gravimetrical method. Although the same amount of nano-$CaCO_3$ and St was used in all the reaction systems, the content of nano-$CaCO_3$ in the prepared nanocomposites changed from 15.4 to 20.4% and the monomer conversion varied from 58.6 to 78.2%.

Characterization

FTIR spectroscopic analyses of the samples were performed on a NEXUS 670 spectrometer (USA) at the wavenumber range of 400–4000 cm^{-1}. The molecular weight and molecular weight distribution of the polymer in the nanocomposite were determined by gel permeation chromatography (GPC). The samples used for GPC measurements were obtained through the Soxhlet extraction with tetrahydrofuran (THF). The GPC was conducted on a Waters Breeze GPC equipped with a Waters 1515 HPLC pump, a Waters 2414 refractive index detector, and three Waters Styragel high-resolution columns (HR4, HR2, and HR1). The system was calibrated with PS standards, and THF was used as an eluent at a flow rate of 1 mL/min.

Thermal analyses were carried out using a differential scanning calorimetry (DSC) Q-50 (TA Instruments). Material was heated from room temperature to 180°C at a rate of 20°C/min and kept isothermal for 3 min to remove the thermal history, and then, it was quenched to 0°C and heated again from 0 to 180°C at a rate of 10°C/min under nitrogen. The glass transition temperature was determined as the temperature corresponding to half the step increase in the heat capacity.

The rheological properties of the samples were measured at 170°C by means of AR50 Rheometer (TA Instruments) using parallel plates of 40 mm diameter. Complex viscosity, storage modulus, and loss modulus as a function of frequency were measured using the dynamic oscillatory mode. Frequency sweep experiments were carried out at the strain level of 5% and the angular frequency range of 2–100 rad/s.

The phase morphologies of the composites were examined using a Jeol JSM-5600LV scanning electron microscope. Samples were fractured in liquid nitrogen. The fracture surfaces were sputtered with gold.

Small-angle X-ray scattering (SAXS) measurements were made using a Philip PW-1700 X-ray diffractometer, at a power of 1.8 KW, with a Cu Kα radiation. The wavelength of the radiation is $\lambda = 0.154$ nm. The samples were scanned in the 2θ range of 0.4°–6° at a scan step of 0.02°. The measured intensity was corrected for air scattering before further analysis. The material was pressed at 170°C in a heated press to obtain a sheet, which was used for SAXS measurement.

Impact testing was carried out using a XJJ-5 impact tester. The composites were compressed at 170°C into sheets, which were then machined into rectangular samples for impact testing.

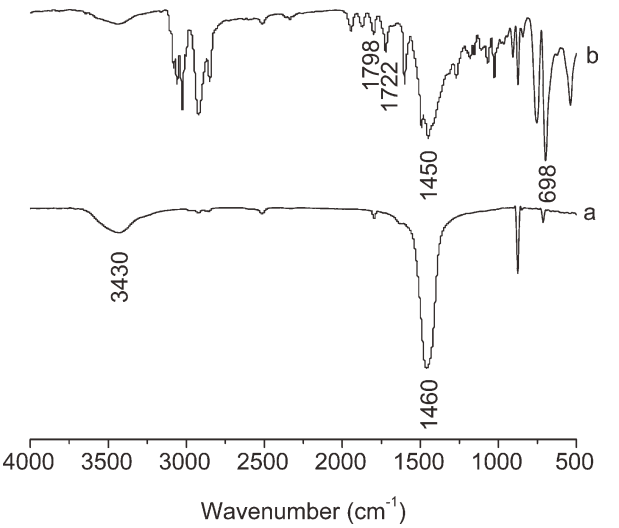

Figure 1. IR spectra of (a) nano-$CaCO_3$ particles and (b) PS/nano-$CaCO_3$ composites with application of MA.

RESULTS AND DISCUSSION

IR Spectra Studies

The Fourier transform infrared (FTIR) spectra of the samples are shown in Figure 1. The IR spectrum of the original nano-$CaCO_3$ (Figure 1, Curve a) exhibits a characteristic absorption band at 1460 cm^{-1}, which is attributed to the C—O stretching vibration. The wide adsorption at 3430 cm^{-1} is accounted for O—H stretching vibration due to physical adsorption water. For the IR spectrum of the PS/nano-$CaCO_3$ composites with MA (Figure 1, Curve b), other than C=C stretching vibrations at 1601, 1492, 1450 cm^{-1} and bending vibration at 698 cm^{-1} of the phenyl group of PS, the characteristic absorption of the carbonyl group of MA at 1798 cm^{-1} is also observed. Because the unreacted MA monomer has been removed from the purified samples, the exhibited absorption band at 1798 cm^{-1} indicates

Table I. Polymerization Results for the PS/Nano-$CaCO_3$ *In Situ* Composites with Varying Content of MA Added After 30 min of Reaction

Sample	[MA]/[St] (mol %)	Monomer conversion (%)	M_n (g/mol)	M_w (g/mol)	M_w/M_n
1	0	58.6	20,980	37,592	1.79
2	4.2	78.2	24,542	45,487	1.85
3	8.4	72.1	23,484	42,676	1.82

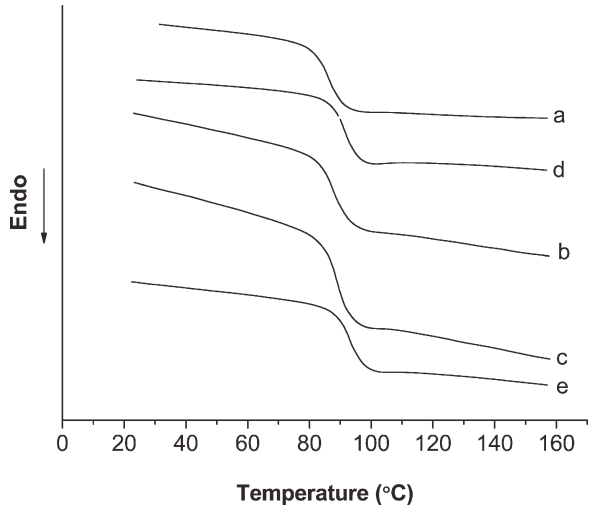

Figure 2. DSC curves of PS/nano-$CaCO_3$ composites with varying content of MA added after 30 min of reaction: (a) 0, (b) 2.1, (c) 4.2, (d) 6.3, and (e) 8.4 mol %.

that the copolymer of St and MA is formed in the composite. The relatively strong absorption at 1722 cm^{-1} is attributed to the carbonyl group of maleic acid, suggesting that most of the MA in the styrene-maleic anhydride (SMA) copolymer exist as carboxylic acid through hydrolysis in aqueous solution.

Molecular Weight of the Polymer in the Composites

The effects of MA content on the monomer conversion and the molecular weight of the polymer in the composites are presented in Table I. When compared with the composite without MA, the *in situ* composites with application of MA have a higher monomer conversion and molecular weight. MA has a little tendency to homopolymerize in free radical polymerization conditions because of the symmetry of the double bond and steric hindrance; however, it can copolymerize with St in the composite as indicated by the FTIR results. The free radical copolymerization of St and MA yields an alternating copolymer.[16–18] The electron-withdrawing characteristic of MA and the electron-donating capacity of St facilitate the formation of charge transfer complex (CTC) between St and MA. The CTC has a far greater reactivity toward the propagating radical when compared with free monomer St and MA,[18,19] leading to an increase in the molecular weight of the polymer in the composites.

DSC Studies

Figure 2 shows the DSC curves of PS/nano-$CaCO_3$ composites with different MA contents. It can be seen that only one glass transition is observed for all the composites. For the composite without application of MA, the glass transition is corresponding to PS. With the addition of MA during the polymerization, PS and copolymers of St with MA are produced. In this work, the amount of MA used is relatively low in comparison with that of St, and therefore, the copolymer has few MA units. Alternating copolymerization of St and MA may take place in the initial stage of the reaction followed by polymerization of pure St after almost complete exhaustion of MA molecules in the reaction

Table II. Glass Transition Temperatures of PS/Nano-$CaCO_3$ Composites

[MA]/[St] (mol %)	Addition time of MA (min)	T_g (°C)
0	30	86.2
2.1	30	87.6
4.2	30	88.9
6.3	30	91.5
8.4	30	93.0
6.3	10	92.4
6.3	120	90.0

system, the possible structure of the copolymer may be as follows[17]:

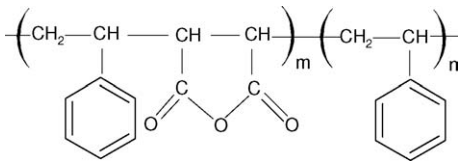

Because of the low content of MA in the copolymer and good miscibility between PS and SMA, the glass transition of PS phase and SMA phase may be superposed and the composites exhibit only one glass transition.

The glass transition temperatures (T_gs) for the PS/nano-$CaCO_3$ *in situ* composites are given in Table II. With the increase of MA content, the PS/nano-$CaCO_3$ composite has a higher T_g. The presence of anhydride rings in the polymer backbone increases the chain rigidity, leading to an increase in the T_g. Additionally, the increase in the molecular weight may have a contribution to the increase in the T_g. In this work, the T_g increases from 86.2 to 88.9°C when the content of MA in the feed increases from 0 to 4.2 mol %, correspondingly the M_w increases from 37,592 to 45,487 g/mol. When the MA content further increases from 4.2 to 8.4 mol %, the M_w has a slight decrease, but the T_g further increases to 93°C. This may be explained by the fact that the

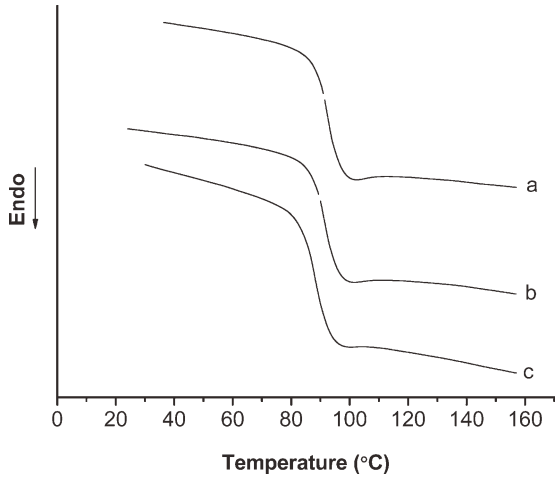

Figure 3. DSC curves of PS/nano-$CaCO_3$ composites with 6.3 mol % of MA added after different time of reaction: (a) 10, (b) 30, and (c) 120 min.

Applied Polymer SCIENCE

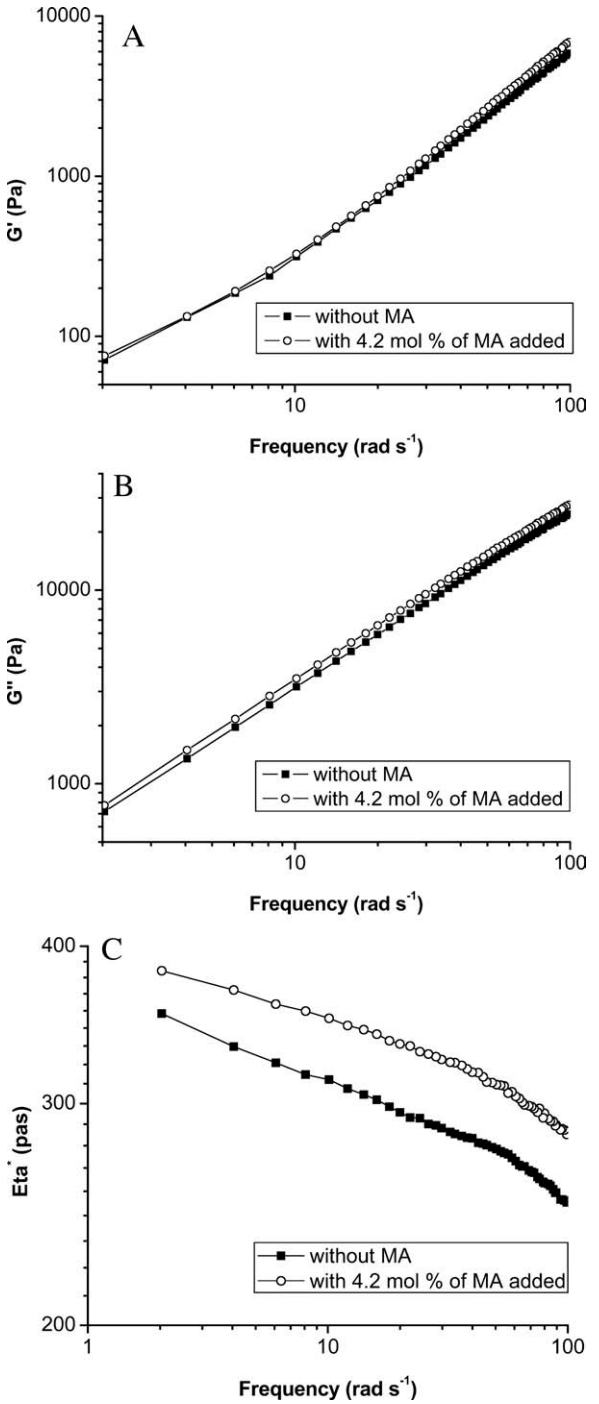

Figure 4. Influence of the application of MA on (A) storage modulus, (B) loss modulus, and (C) dynamic viscosity of PS/nano-$CaCO_3$ composites.

carboxylic acid group in the polymer backbone and Ca ions of $CaCO_3$ can form coordination bonds,[20–22] resulting in an enhanced interfacial adhesion between PS and nano-$CaCO_3$ particles. The increased interfacial interaction has also a contribution to a higher T_g of the composite.

Figure 3 shows the DSC curves of the PS/nano-$CaCO_3$ composites with MA added at different times. Their T_gs are presented in Table II. The later MA is added, the more difficult it is for MA monomers to diffuse into polymer particles for the increasing viscosity of the reaction system. Hence, fewer MA units are introduced into the copolymer, resulting in a lower T_g of the composite.

Rheological Analyses

The viscoelastic properties of polymer/inorganic nanocomposites are associated with their microstructure. Figure 4 shows the complex modulus of the PS/nano-$CaCO_3$ composites as a function of frequency at 170°C. As indicated in Table I, the monomer conversion increases from 58.6 to 78.2% when the content of MA

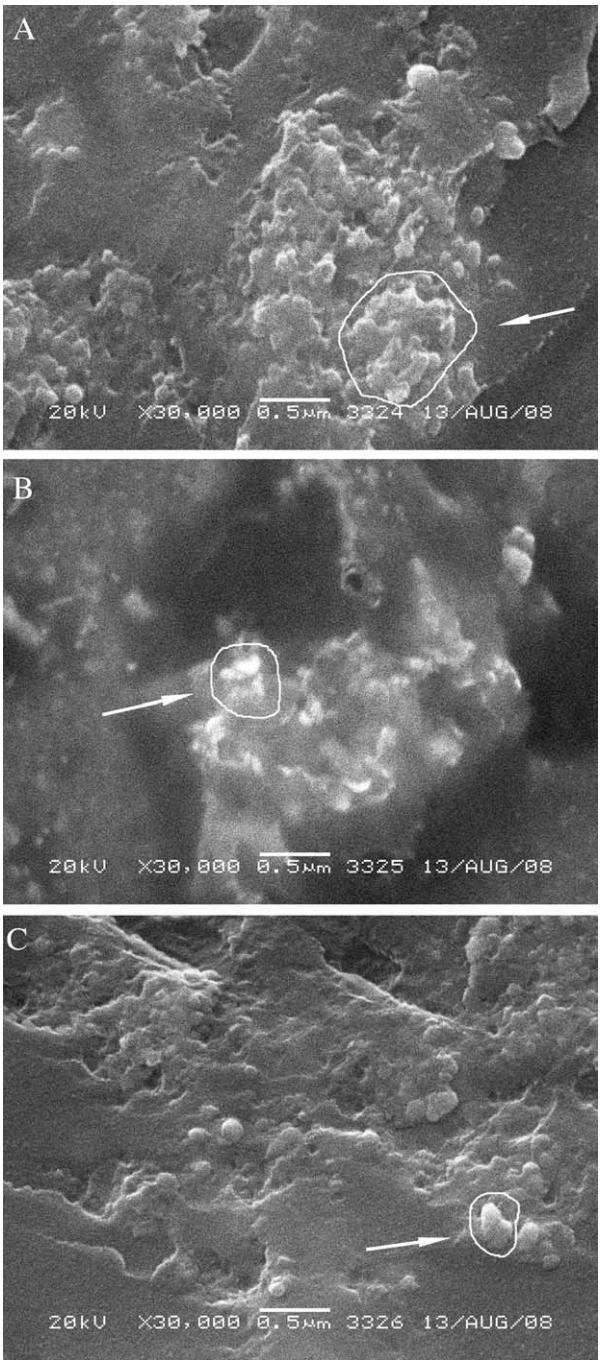

Figure 5. SEM micrographs of PS/nano-$CaCO_3$ composites with varying content of MA added after 30 min of reaction: (A) 0, (B) 2.1, and (C) 4.2 mol %.

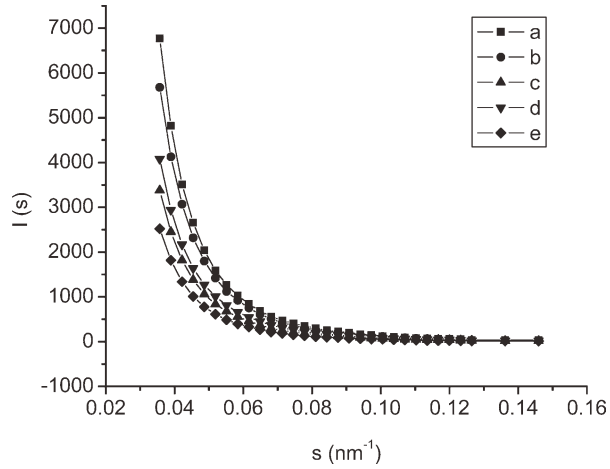

Figure 6. SAXS curves of PS/nano-$CaCO_3$ composites with varying content of MA added after 30 min of reaction: (a) 0, (b) 2.1, (c) 4.2, (d) 6.3, and (e) 8.4 mol %.

increases from 0 to 4.2 mol %. A greater degree of monomer conversion means a higher polymer content or lower nano-$CaCO_3$ content in the composite because the same amount of nano-$CaCO_3$ is used in all the reaction systems. A lower content of inorganic nanoparticles in the polymer nanocomposite usually leads to a lower complex modulus of the composite.[23,24] In this work, however, the composite with a lower content of nano-$CaCO_3$ in the presence of MA shows a higher storage modulus, loss modulus, and dynamic viscosity in comparison with the composite in the absence of MA, especially at large frequency. The increase in the complex modulus may be ascribed to the increased molecular weight of the polymer and the improved interfacial adhesion between the polymer and nano-$CaCO_3$ particles.

Morphology

Figure 5 shows scanning electron microscope (SEM) images of PS/nano-$CaCO_3$ composites with different contents of MA. Some big agglomerates of $CaCO_3$ nanoparticles can be seen in the composite without MA [Figure 5(A)]. However, there are not only much fewer but also smaller agglomerates in the composites with the application of MA [Figure 5(B,C)], indicating that the application of only a small amount of MA can effectively improve the dispersion of $CaCO_3$ nanoparticles in the polymer matrix. This may be ascribed to the improved compatibility between the polymer and nano-$CaCO_3$ particles.

More information about the microstructure can be obtained from the SAXS curves of the composites, as shown in Figure 6. The SAXS intensity of the composite with application of MA is lower than that without MA, indicating that a finer and more homogeneous microstructure of PS/nano-$CaCO_3$ composite is achieved in the presence of MA. For random heterogeneous media, the intensity of scattering, $I(s)$, can be expressed as follows[25]:

$$I(s) = k\langle\eta^2\rangle \int_0^\infty \gamma(r)\frac{\sin(sr)}{sr}r^2 dr, \quad (1)$$

where K is a proportional constant, $s = (2\sin\theta)/\lambda$, λ is the wavelength of incident X-ray, θ is the incident angle, $\gamma(r)$ is the correlation function and can be presented as

Table III. Correlation Distance and Porod Invariant of PS/Nano-$CaCO_3$ Composites with Varying Content of MA Added After 30 min of Reaction

[MA]/[St] (mol %)	a_c	Q
0	76.3	1.195
2.1	68.1	1.028
4.2	62.0	0.538
6.3	65.6	0.629
8.4	55.5	0.429

$$\gamma(r) = \exp(-r/a_c), \quad (2)$$

where a_c is named as the correlation distance and defines the size of heterogeneity. For dilute discrete droplets, a_c is related to the drop size. If eq. (2) is substituted into eq. (1), one obtains the following equation:

$$I(s)^{-1/2} = \left[k'\langle\eta^2\rangle a_c^3\right]^{-1/2}\left(1 + s^2a_c^2\right) \quad (3)$$

a plot of $I(s)^{-1/2}$ versus s^2 should lead to a straight line, and the ratio of the slope to the intercept is equal to a_c^2.

The correlation distance of PS/nano-$CaCO_3$ composites with different contents of MA is given in Table III. It is found that, with the increase of MA content, the correlation distance decreases, denoting a finer dispersion of $CaCO_3$ particles. This is consistent with the results of SEM measurements.

According to Porod's law,[26] the Porod invariant Q, which is used to describe inhomogeneity of a system, can be presented as

$$Q = \int_0^\infty s^2 I(s) ds \quad (4)$$

The Porod invariants with various MA contents for PS/nano-$CaCO_3$ composites are presented in Table III. As shown in Table III, the Porod invariant decreases with the increase of MA content, indicating that the addition of MA improves the homogeneity of the PS/nano-$CaCO_3$ composites.

Mechanical Properties

The influence of MA content on impact strength of the composites is illustrated in Table IV. It can be seen that the PS/nano-$CaCO_3$ *in situ* composites in the presence of MA have a higher impact strength when compared with the composite in the absence of MA. The increase in impact strength may be attributed to the increased molecular weight of the polymer, the enhanced

Table IV. Impact Strength of PS/Nano-$CaCO_3$ Composites with Varying Content of MA Added After 30 min of Reaction

[MA]/[St] (mol %)	Impact strength (kJ/m^2)
0	0.852
2.1	1.141
4.2	1.349
6.3	1.005
8.4	1.205

interfacial adhesion between the polymer and nano-$CaCO_3$ particles, and the improved dispersion of nanoparticles with the addition of MA into the composite.

CONCLUSIONS

The copolymer of St and MA is formed during the preparation of PS/nano-$CaCO_3$ *in situ* composites by adding a small amount of MA and acts as a compatibilizing agent for PS and $CaCO_3$ nanoparticles. The glass transition temperature, complex modulus, and impact strength of the PS/nano-$CaCO_3$ composites show an increase with the addition of MA. The addition of the anhydride group to the polymer also improves the dispersion of calcium carbonate nanoparticles in the polymer matrix.

ACKNOWLEDGMENTS

Contract grant sponsor: Hunan Provincial Natural Science Foundation of China; Contract grant number: 09JJ6076.

REFERENCES

1. Homminga, D.; Goderis, B.; Groeninckx, G.; Reynaers, H.; Hoffman, S. *Polymer* **2005,** *46*, 9941.
2. Lee, C. U.; Dadmun, M. D. *J. Polym. Sci. Part B: Polym. Phys.* **2008,** *46*, 1747.
3. Suhr, J.; Joshi, A.; Schadler, L.; Kane, R. S.; Koratkar, N. A. *J. Nanosci. Nanotech.* **2007,** *7*, 1684.
4. Scott, M.; Victor, A. K.; Steve, S. *Polymer* **2008,** *49*, 757.
5. Kaminsky, W.; Wiemann, K. *Expected Mater. Future.* **2003,** *3*, 6.
6. Funck, A.; Kaminsky, W. *Compos. Sci. Technol.* **2007,** *67*, 906.
7. Hu, N. T.; Zhou, H. W.; Dang, G. D.; Rao, X. H.; Chen, C. H.; Zhang, W. J. *Polym. Int.* **2007,** *56*, 655.
8. Han, S. I.; Lim, J. S.; Kim, D. K.; Kim, M. N.; Im, S. S. *Polym. Degrad. Stab.* **2008,** *93*, 889.
9. Cui, L. Q.; Tarte, N. H.; Woo, S. I. *Macromolecules* **2008,** *41*, 4268.
10. Hwang, S. Y.; Lee, W. D.; Lim, J. S.; Park, K. H.; Im, S. S. *J. Polym. Sci. Part B: Polym. Phys.* **2008,** *46*, 1022.
11. Scharlach, K.; Kaminsky, W. *Macromol. Symp.* **2008,** *261*, 10.
12. Zeng, H. L.; Gao, C.; Wang, Y. P.; Watts, P. C. P.; Kong, H.; Cui, X. W.; Yan, D. Y. *Polymer* **2006,** *47*, 113.
13. Ma, C.; Rong, M.; Zhang, M.; Friedrich, K. *Polym. Eng. Sci.* **2005,** *45*, 529.
14. Bagwe, R. P.; Hilliard, L. R.; Tan, W. *Langmuir* **2006,** *22*, 4357.
15. Zhou, X. P.; Xie, X. L.; Yu, Z. Z.; Mai, Y. W. *Polymer* **2007,** *48*, 3555.
16. Doiuchi, T.; Kubouchi, K.; Minoura, Y. *Macromolecules* **1977,** *10*, 1208.
17. Szalay, J.; Nagy, I.; Bányai, I.; Deák, G.; Bazsa, G.; Zsuga, M. *Macromol. Rapid Commun.* **1999,** *20*, 315.
18. Qiu, G. M.; Zhu, B. K.; Xu, Y. Y.; Gekeler, K. E. *Macromolecules* **2006,** *39*, 3231.
19. Hill, D. J. T.; O'Donnell, J. H.; O'Sullivan, P. W. *Macromolecules* **1985,** *18*, 9.
20. Rivas, B. L.; Pooley, S. A.; Pereira, E.; Montoya, E.; Cid, R. *J. Appl. Polym. Sci.* **2006,** *101*, 2057.
21. Amaro, L. P.; Rivas, B. L.; Coiai, S.; Passaglia, E.; Augier, S.; Ciardelli, F. *J. Appl. Polym. Sci.* **2009,** *113*, 290.
22. Albu, A. M.; Mocioi, M.; Mateescu, C. D.; Iosif, A. *J. Appl. Polym. Sci.* **2011,** *121*, 1867.
23. Otsubo, Y.; Umeya, K. *J. Rheol.* **1984,** *28*, 95.
24. Tang, Y. H.; Yang, C.; Gao, P.; Ye, L.; Zhao, C. B.; Lin, W. *Polym. Eng. Sci.* **2011,** *51*, 133.
25. Mo, Z. S.; Zhang, H. F. Structure of Crystalline Polymers by X-ray Diffraction; Science Press: Beijing, **2003.**
26. Porod, G.; Koll, Z. Z. *Polymer* **1952,** *125*, 51.